Lab on a Chip

PAPER

High-throughput biophysical measurement of human red blood cells†

Yi Zheng,[ab] **Ehsan Shojaei-Baghini,**[a] **Azar Azad,**[d] **Chen Wang**[*de] **and Yu Sun**[*abc]

This paper reports a microfluidic system for biophysical characterization of red blood cells (RBCs) at a speed of 100–150 cells s^{-1}. Electrical impedance measurement is made when single RBCs flow through a constriction channel that is marginally smaller than RBCs' diameters. The multiple parameters quantified as mechanical and electrical signatures of each RBC include transit time, impedance amplitude ratio, and impedance phase increase. Histograms, compiled from 84,073 adult RBCs (from 5 adult blood samples) and 82,253 neonatal RBCs (from 5 newborn blood samples), reveal different biophysical properties across samples and between the adult and neonatal RBC populations. In comparison with previously reported microfluidic devices for single RBC biophysical measurement, this system has a higher throughput, higher signal to noise ratio, and the capability of performing multi-parameter measurements.

Introduction

Because of the physiological and pathological importance of RBCs, their biophysical properties (mechanical and electrical properties) have been under intensive study over the past decades.[1–3] The mechanical property of RBCs is essentially determined by the membrane skeleton, and the interaction between the membrane skeleton and membrane integral proteins.[4,5] RBCs' exceptional capacity to deform is of crucial importance to both macro and microcirculation. The high deformability of normal RBCs enables them to pass capillaries that are smaller than the diameter of RBCs. A range of diseases have been described in association with impaired RBC deformability, such as sepsis,[6,7] malaria,[8,9] sickle cell anemia (hemoglobin disorder),[10,11] and myocardial ischaemia and microvascular dysfunction.[12] In the meanwhile, the electrical properties of RBCs have also been correlated to pathological conditions.[13–15] For example, the ion channel conductance of malaria parasite infected RBCs is lower than the uninfected RBCs due to the blockage of ion channels by the parasites.[16]

A number of technologies have been used for measuring single RBC's biophysical properties,[17,18] for instance, micropipette aspiration,[19] atomic force microscopy,[20,21] and optical tweezers[22,23] for mechanical measurement and patch-clamping for electrical measurement.[14,16] However, these technologies are difficult to use and have a low testing speed. The heterogeneity of RBCs within a sample demands a higher testing throughput in order to obtain statistically significant data, and thus, determine RBCs' genuine mechanical and electrical properties.

Microfluidic technologies have gained momentum in single RBC biophysical characterization.[9,24,25] Microchannels were used to generate fluid stress for investigating membrane viscoelastic properties of RBCs. Deformation index was quantified using high-speed imaging as an indicator of RBCs' deformability.[26] Bow *et al.* recently reported a deformability-based RBC testing device using constriction channels. Resulting flow velocities were used to distinguish malaria infected RBCs from normal RBCs.[8] Microfluidic devices have also been employed to mechanically characterize individual RBCs by examining the duration needed for electroporation induced lysis.[27]

Microfluidic devices for single-cell electrical measurement were also developed based on micro patch-clamping,[28–31] electrorotation[32,33] and impedance flow cytometry.[34,35] Patch-clamping characterizes cellular electrical properties by aspirating a cell membrane patch into a microchannel to form a high electrical resistance seal. Due to the rectangular-like shape of microchannels and the high deformability of RBCs, aspirating only a patch of the RBC membrane (*vs.* sucking whole RBCs into a microchannel) is difficult to realize on micro patch-clamping devices. Electrorotation was previously used for RBC measurement;[32] however, it is difficult to achieve efficient rotation in high conductivity physiological buffer, and throughput is extremely low. Impedance flow cytometry[34,35] has recently been reported for single-cell impedance measurement as well as for electrical property characterization of single RBCs.[36,37] The

[a] Department of Mechanical and Industrial Engineering, University of Toronto, Toronto, ON, M5S 3G8, Canada. E-mail: sun@mie.utoronto.ca; Fax: +1-416-978-7753; Tel: +1-416-946-0549
[b] Institute of Biomaterials and Biomedical Engineering, University of Toronto, Toronto, ON, M5S 3G8, Canada
[c] Department of Electrical and Computer Engineering, University of Toronto, Toronto, ON, M5S 3G4, Canada
[d] Department of Pathology and Laboratory Medicine, Mount Sinai Hospital, Toronto, Canada
[e] Department of Laboratory Medicine and Pathobiology, University of Toronto, Toronto, Canada. E-mail: cwang@mtsinai.on.ca; Tel: +1-416-586-4469
† Electronic supplementary information (ESI) available. See DOI: 10.1039/c2lc21210b

reported technique suffered from current leakage, which can cause small electrical differences across RBCs to be unobservable, making it unsuitable for distinguishing electrical properties of different RBC populations.

This paper presents a microfluidic system for simultaneous mechanical and electrical characterization of single RBCs. Detection involves only electrical signals and has a throughput of 100–150 cells per second. Since adult and fetal/neonatal RBCs are known to be different in size and hemoglobin contents, we applied our system to test RBCs in adult blood (~16,000 cells per sample, 5 samples) and neonatal RBCs (~16,000 cells per sample, 5 samples) and revealed their differences in mechanical and electrical properties. We also explored the utility of biophysical (mechanical and electrical) data for distinguishing neonatal RBCs from adult RBCs. We previously reported impedance measurement on single cells.[38,42] In this study, cell measurement speed has been improved significantly (100–150 cells s^{-1} vs. ~1 cell s^{-1} as in our previous work). Data analysis methods are developed for reliably distinguishing RBCs, WBCs (white blood cells) and platelets within full blood samples. Correlations between cell volume, hemoglobin density, and RBC biophysical properties, for the first time, are established quantitatively.

System overview

Fig. 1(a) shows the schematic diagram of the single RBCs biophysical characterization system. The microfluidic chip was constructed by bonding PDMS microchannels on a glass slide. Two Ag/AgCl non-polarizable electrodes were connected to the function generator (sinusoidal voltage at 100 kHz @1.0 V$_{pp}$) and the lock-in amplifier (SR850, Stanford Research Instruments, USA) and inserted into the inlet and outlet ports of the microfluidic device. The analog outputs of the lock-in amplifier were sampled with a 16-bit DAQ card (NI PCI-6229, National Instruments, USA) and data capture software (LabVIEW, National Instruments, USA). Dilute blood sample was pipetted into the inlet reservoir of the device and driven through the constriction channel by hydraulic pressure difference (see Fig. 1(b)).

Fig. 1(c) shows the equivalent circuit model. The channel is equivalent to a resistor $R_{channel}$ and a capacitor $C_{channel}$ connected in parallel.[38] As a RBC (including membrane capacitance C_{cell} and cytoplasm resistance R_{cell})[39,40] passes through the constriction channel, it perturbs the electric field in the volume within the channel and generates a current impulse. R_{leak} represents the sealing resistance between the RBC membrane and channel walls. In the mean time, the current change of the circuit loop is sensed via input impedance (I_{inner}) of the lock-in amplifier (10 MΩ + 25 pF), amplified and recorded by the data capture software. Outputs of the lock-in amplifier consist of the real component (X) and the imaginary component (Y). The amplitude (A) and phase (Φ) were calculated according to $A = \sqrt{X^2 + Y^2}$, $\Phi = \arctan\left(\dfrac{Y}{X}\right)$. An algorithm was used to extract the transit time (the time duration taken by a cell to travel through the constriction channel, ΔT), the amplitude ratio (the ratio between the lowest amplitude value captured when the cell squeezes
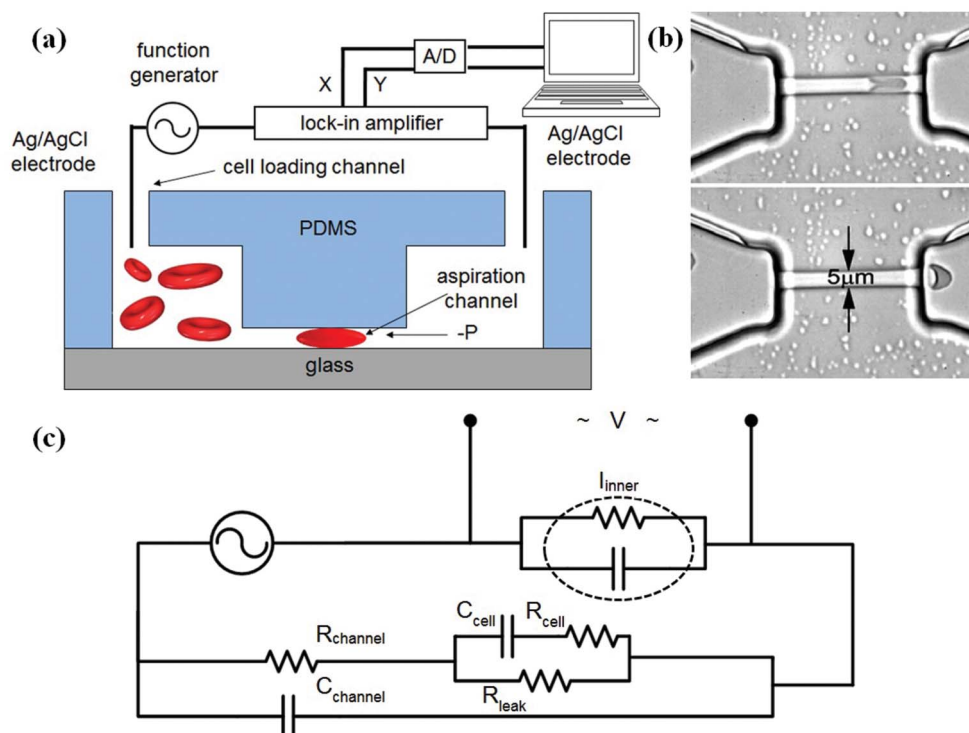

Fig. 1 (a) Schematic of the microfluidic system for electrical and mechanical characterization of RBCs. Two Ag/AgCl non-polarizable electrodes are connected to a function generator (100 kHz @1.0 V$_{pp}$) and a lock-in amplifier. The two electrodes are inserted into the inlet and outlet ports of the device. As RBCs are aspirated through the constriction channel, electrical current change is sensed and amplified. "$-P$" denotes the negative pressure used to aspirate RBCs through the constriction channel. (b) Measurements are made when an RBC passes through the constriction channel. (c) Equivalent circuit model of the system.

through the constriction channel and the amplitude value with no cell in the constriction channel, $(A - \Delta A)/A)$, and the phase difference between with cells and without cells $(\Delta \Phi)$.

Compared with previously reported microfluidic devices for biophysical measurements, this design has a few advantages. Firstly, almost all electrical field lines are forced to penetrate RBCs' membrane and hemoglobin inside, making the device more sensitive to minute biophysical differences. Secondly, our measurement is purely electrical, eliminating the need for microscopy imaging and hence, permitting high measurement throughputs. High-speed cameras (tens of kHz) generate gigabyte data per second and can only record for a few seconds due to limited memory. Processing massive amounts of image data also takes tremendous computation efforts and time. Therefore, for microfluidic single cell measurement systems, high-speed imaging offers high speeds, but the total number of data points (*i.e.*, sample size) is limited.[27,41] Thirdly, no sheath flow is required on our device. Since the constriction channel's cross-sectional area is smaller than the diameter of RBCs, only a single RBC is permitted to pass through the constriction channel in a given time instance simply by tuning the density of the RBC suspension.

Materials and methods

Device fabrication

The constriction channel (first layer) was fabricated with SU8-2002 (5 μm × 3 μm) (MicroChem Corp., Newton, MA, USA) on a glass slide. A second layer of SU8-25 was then spin coated on the glass slide covered with the first layer features, soft-baked, and exposed to UV light with alignment, followed by post-exposure bake, development and hardbake. The loading channel's cross-sectional area (1000 μm × 30 μm) is much larger than that of the constriction channel. Hence, the impedance of the device is mainly determined by the constriction channel. The microchannels were molded with PDMS (Ellsworth Adhesives, ON, Canada), punched to form inlet and outlet ports, and bonded to a glass slide treated with a corona-treater (Electro-Technic Products Inc., Illinois, USA).

Blood samples and experimental protocol

Peripheral blood samples were obtained following routine blood tests at the hospital hematology laboratory. Blood samples were collected using commercial vacuum tubes with EDTA anticoagulant (ethylenediaminetetraacetic acid 1.5 mg ml^{-1}) (Sigma-Aldrich, Oakville, ON, Canada). The adult ($n = 5$) and newborn samples ($n = 5$) were of normal individuals with the complete blood counts performed by a standard commercial hematology analyzer (Sysmex XE-2100, Kobe, Japan). Hematologic information of all 10 samples is summarized in the electronic supplementary information (ESI) Table S.1.† In the experiments, 10 μL blood was diluted in 500 μL PBS (Sigma-Aldrich, Oakville, ON, Canada) mixed with 0.2% w/v Pluronic (Sigma-Aldrich, Oakville, ON, Canada) and 1% w/v BSA (New England Biolabs Inc., Herts, UK). Pluronic and BSA were used for
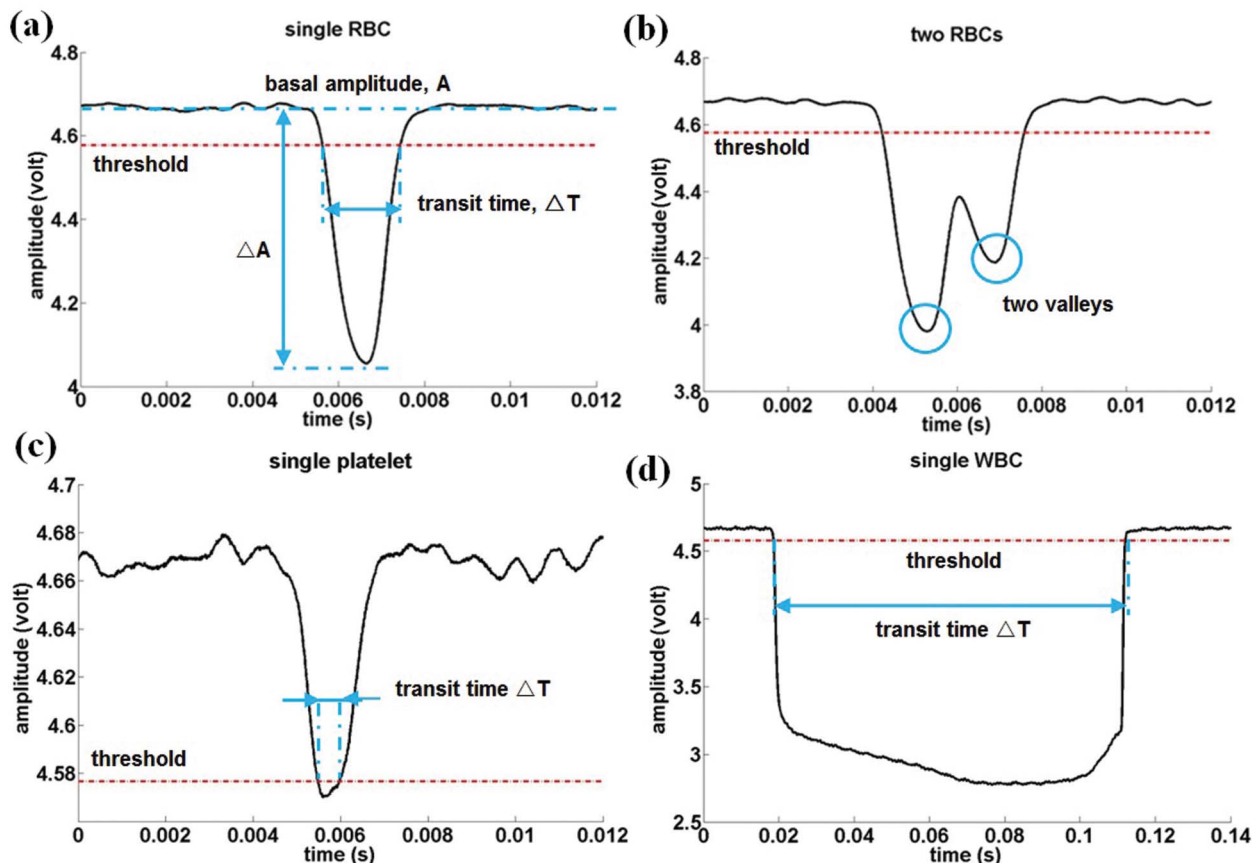

Fig. 2 Experimental amplitude profiles: (a) a single RBC, (b) two RBCs, (c) a single platelet, and (d) a single WBC within the constriction channel.
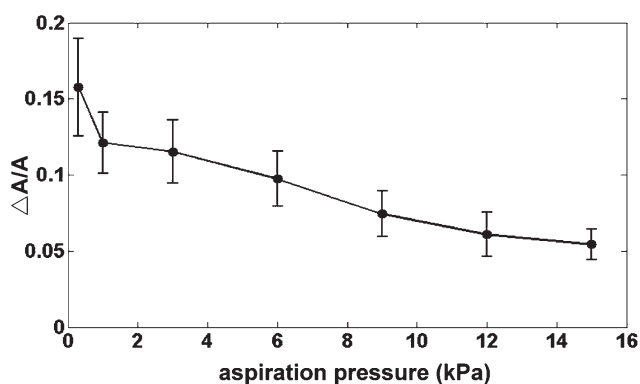
Fig. 3 Ratio of the amplitude change and the basal amplitude *vs.* aspiration pressure. Device sensitivity becomes lower at higher aspiration pressure due to RBC deformation and larger leakage current.

preventing non-specific adhesion to the channel walls. The dilute samples were placed for 20 min before usage. Before the sample was pipetted into the inlet port of the device, the microchannel was filled with PBS solution with 0.2% w/v Pluronic and 1% w/v BSA. A pressure difference (50 Pa) between the inlet and outlet ports was applied for 30 min to ensure the equilibrium in lubrication of the channel walls. A 5 µL dilute blood suspension was then pipetted into the entrance of the cell loading channel. The two Ag/AgCl non-polarizable electrodes were inserted into the inlet and outlet ports of the device. A negative pressure of 3 kPa was then applied to aspirate cells continuously through the constriction channel while electrical data was sampled.

Electrical measurement and data analysis

A sinusoidal voltage (100 kHz @1.0 V_{pp}) was applied to the two Ag/AgCl electrodes. When an RBC is aspirated into the constriction channel, it blocks electric field lines and causes the current in the circuit loop to drop. During experiments, the real component (X) and the imaginary component (Y) of the lock-in amplifier output were sampled at 120 kHz. X and Y were converted to amplitude (A) and phase (Φ). Fig. 2 shows amplitude profiles of a single RBC, two RBCs, a single platelet, and a single WBC within the constriction channel (phase profiles are presented in the ESI,† Fig. S.1).

The present throughput of our system is 100–150 cells s^{-1}. The variation in throughput depends on cell density differences across patient samples. Fig. S.2† shows an example set of raw measurement data. A threshold is defined as 98% of the basal amplitude (the amplitude without cell presence in the constriction channel) (see Fig. 2(a)). Comparing a signal and the threshold amplitude value, the portions where the signal's amplitude is lower than the threshold value were considered as cell passage regions. A quadratic polynomial peak detector was used to detect the valleys within the cell passage regions. The time period between the two intercepts with the threshold value was interpreted as cell transit time (ΔT), which is determined by the cell's size and mechanical stiffness. The amplitude ratio (($A - \Delta A)/A$) (see Fig. 2(a)) and the phase increase ($\Delta \Phi$) (see ESI,† Fig. S.1(a)) were quantified as the cell's electrical signatures. If the transit time of a region is longer than 20 ms (*vs.* ∼2 ms for RBCs), this region is known to be caused by the passage of a WBC and excluded from the RBC data. Meanwhile, more than one valley within a cell passage region suggests the passage of more than one cell (see Fig. 2(b)). Since the electrical field lines are highly concentrated by the constriction channel to penetrate the cell, the electrical signal generated by a single RBC in our experiments was readily distinguishable from the background noise (SNR ⩾ 29 dB). No preamplifier and additional filters were required.
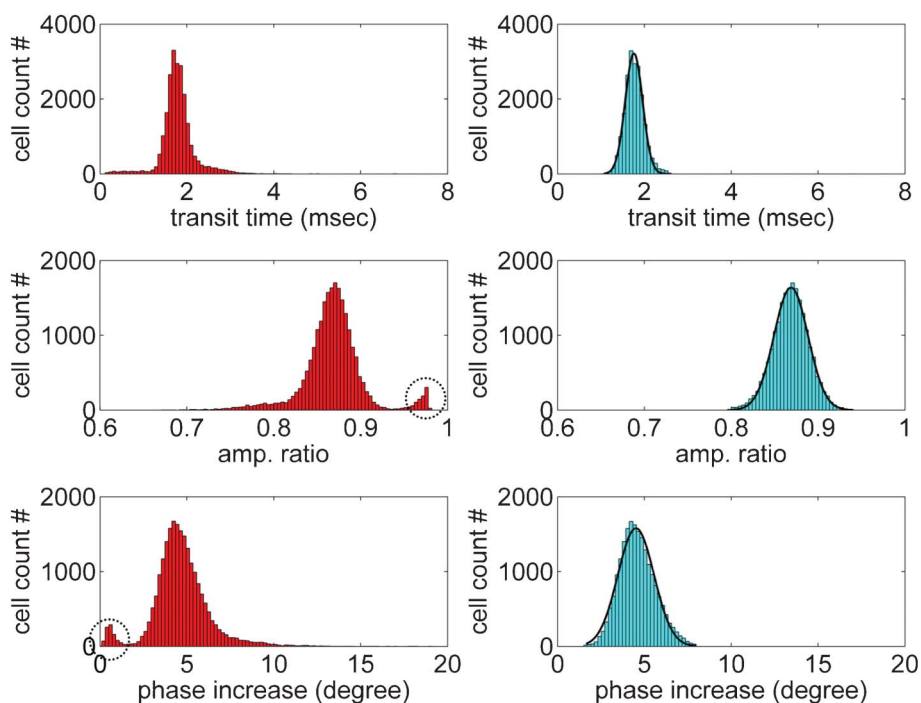

Fig. 4 Histograms of transit time, amplitude ratio and phase increase attained from an adult sample (22 669 cells measured) before (red) and after (cyan) the exclusion of platelets and debris. Circled populations are platelets and debris.
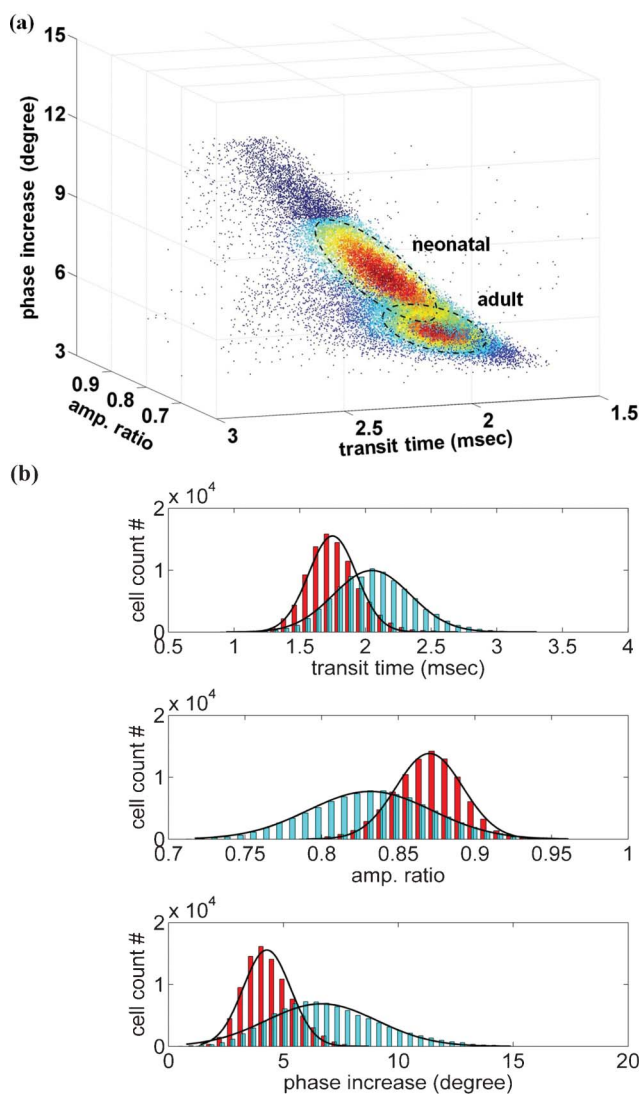
Fig. 5 Adult RBCs (n = 84,073 from 5 adult samples, red), neonatal RBCs (n = 82,253 from 5 newborn samples, cyan). (a) 3D scatter plot of transit time *vs.* amplitude ratio *vs.* phase increase. (b) Histograms of transit time, amplitude ratio, and phase increase fitted with normal distributions. Circled populations are platelets and debris.

Results and discussion

Selection of channel dimension, signal frequency, and applied pressure

Constriction channels having a smaller cross-sectional area can form a better seal between the RBC membrane and the channel walls. However, RBCs collapsed when the cross-sectional area was much smaller than RBCs' diameter. Fig. S3† summarizes the behavior we experimentally observed when RBCs were aspirated through the constriction channel. For constriction channels with a cross-sectional area of 1 μm × 3 μm, almost 100% RBCs collapsed at the entrance of the constriction channel (Fig. S3(a)†). For constriction channels with a cross-sectional area of 2 μm × 5 μm, the majority of RBCs were elongated and then collapsed within the constriction channel (Fig. S3(b)†). For constriction channels with a cross-sectional area of 3 μm × 5 μm

(chosen for our experiments), all RBCs showed folded morphology, and no RBCs collapsed (Fig. S.3(c), video S.1†).

RBCs are highly deformable. The cell shape in the constriction channel is altered by fluid shear stress. At higher aspiration pressures, RBCs are further deformed in the shear stress direction, resulting in a poorer seal between the RBC membrane and constriction channel walls. Consequently, signal change with and without the presence of a cell in the constriction channel becomes smaller due to larger leakage current. Fig. 3 shows the ratio of the amplitude change and the basal amplitude, measured on the same blood sample at different aspiration pressures. Each data point in the figure is from approximately 1,000 cells. In our subsequent experiments, 3 kPa was chosen for a balance between throughput and detection sensitivity. At this aspiration pressure, the velocity of the fluid in the constriction channel is approximately 30 mm s^{-1}. As to frequency selection, the frequency should be high enough to enable the electrical field lines to penetrate the RBC membrane such that the electrical property of RBCs can be reflected by the measured electrical signal. Additionally, the frequency should not be too high. Too high a frequency would result in extremely low impedance of $C_{channel}$ (see Fig. 1(c)) and make electrical field lines undesirably obviate the cell in the constriction channel.[38,42] We experimentally selected 100 kHz for subsequent experiments.

WBCs and platelets

Although RBCs represent over 90% of blood cells, white blood cells (WBCs) and platelets remained in the raw blood samples. WBCs and platelets were excluded in data processing. As shown in Fig. 2, electrical signals measured from RBCs, WBCs, and platelets are drastically different, thus using amplitude ratio alone proved highly effective to distinguish WBCs and platelets from RBCs.

Fig. 4 shows histograms attained from an adult blood sample (22,669 cells measured). The red colored histograms show data after the exclusion of WBCs. The relatively small population (circled) within the blood sample barely perturbed the electrical field lines. This population was made up of platelets and debris that have diameters smaller than 3 μm. The "cyan" data in Fig. 4 are transit time, amplitude ratio, and phase increase with fitted normal distributions after excluding platelets and debris.

RBC measurements

Our microfluidic system (frequency: 100 kHz, pressure difference: 3 kPa, constriction cross-section area: 3 μm × 5 μm) tested adult RBCs (5 samples, ~16,000 cells per sample) and neonatal RBCs (5 samples, ~16,000 cells per sample). As discussed earlier, WBCs and platelets were easily distinguished from RBCs using their distinct transit time and amplitude ratio. Additionally, the analysis of experimental data confirmed that multiple-valley events account for less than 5% of the total events, indicating the occurrence of two or more RBCs (*vs.* single RBCs) inside the constriction channel simultaneously was rare (<5%). Fig. 5(a) shows the 3D scatter plot of transit time *vs.* amplitude ratio *vs.* phase increase of all tested adult RBCs (n = 84,073 from 5 adult samples) and neonatal RBCs (n = 82,253 from 5 newborn samples). The ellipses in the figure track the standard deviation of the distribution. Each of the three
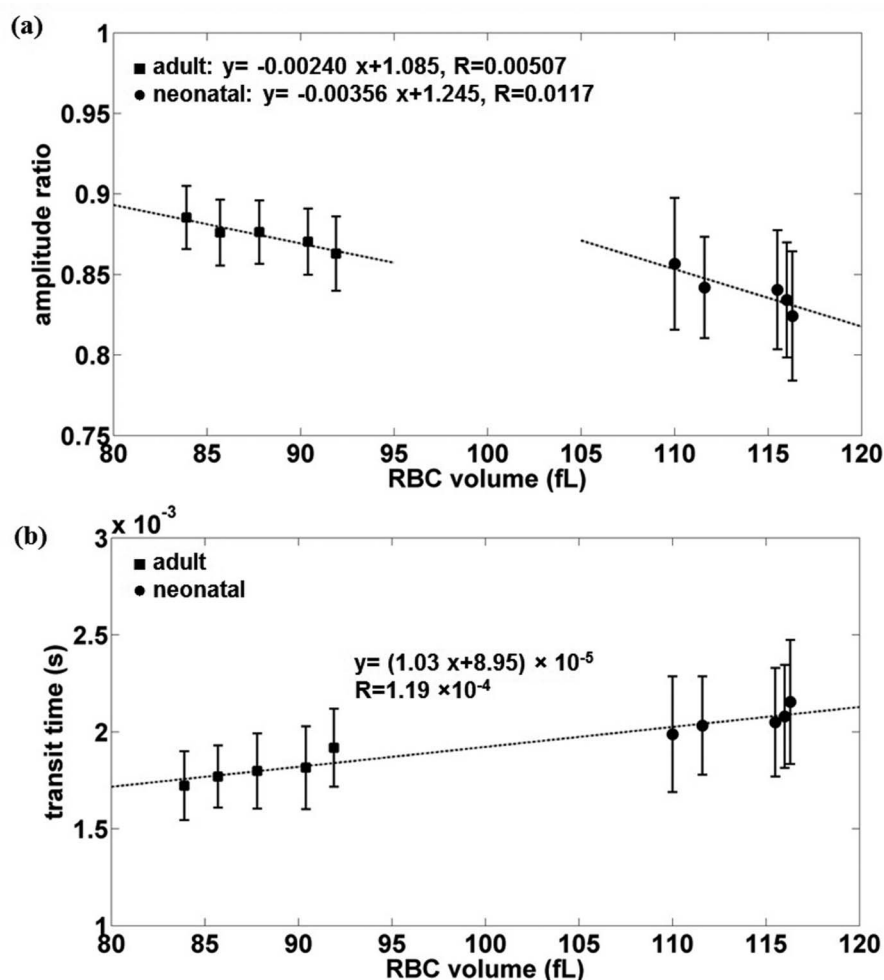
Fig. 6 (a) Amplitude ratio as a function of RBC volume. (b) Transit time as a function of RBC volume.

parameters was identified and fitted to normal distribution profiles (see Fig. 5(b)). Histograms of individual samples are presented in the ESI Fig. S.4.†

A back propagation neural network was used for pattern recognition (MATLAB, MathWork, USA). The input data have three groups of parameters (transit time, amplitude ratio, and phase increase) measured on RBCs. The complete dataset was divided into training data (70%), validation data (15%), and testing data (15%) to quantify adult *vs.* neonatal RBC classification success rates (*i.e.*, accuracy). RBC classification success rates were 76.2% (transit time + amplitude ratio), 78.1% (amplitude ratio + phase increase), 77.9% (phase increase + transit time), and 84.8% (amplitude ratio + phase increase + transit time), suggesting multiple parameters (transit time, amplitude ratio and phase increase), when used in combination, can provide a higher cell classification success rate. Besides the success rate of 84.8%, sensitivity (true positive/(true positive + false negative)) and specificity (true negative/(true negative + false positive)) were 80.2% and 89.2%, respectively (see ESI Fig. S.5†).

Cell transit time is determined by RBCs' volume, membrane stiffness, and the friction between the membrane and channel walls. The electrical impedance amplitude ratio and phase increase are determined by RBCs' volume, ion channels on the membrane, and the density of hemoglobin. Hence, transit time, amplitude ratio, and phase increase are not completely independent parameters (*e.g.*, they are all affected by cell volume). The neural network classification results also indicate that all three parameters can reflect unique properties of RBCs, and higher classification success rates were obtained when these parameters were used in combination.

The amplitude change during a cell's passage through the constriction channel is caused by the blockage of the electrical field lines. Fig. 6(a) reveals a linear trend between the amplitude ratio and the cell volume for both adult RBCs and neonatal RBCs with different slopes (-0.0024 *vs.* -0.00356). Cell electrical properties are determined by membrane capacitance and the resistance of cytoplasm (hemoglobin in the case of RBCs). Since the lipid layer composition of neonatal RBCs and adult RBCs is very similar[43] and the effective area of the membrane capacitance is constricted by the cross section of the constriction channel, the different slopes indicate different conductivity between neonatal RBCs and adult RBCs. This can possibly be related to the higher hemoglobin density inside neonatal RBCs (see ESI Table S.1†). The average RBC volume and hemoglobin density of each sample were obtained from complete blood counts performed by a commercial hematology analyzer (see ESI Table S.1†).

As shown in Fig. 6(b), transit time as a function of RBC volume can be fitted into a single line for both adult RBCs and neonatal RBCs. The transit time of RBCs under a constant negative pressure is determined by the friction force between the membrane and channel walls (friction force = contact pressure × contact area × friction coefficient, where contact pressure is related to membrane stiffness and friction coefficient is related to membrane composition). It is known that the lipid layer composition and membrane stiffness of neonatal and adult RBCs are very close.[43,44] Hence, contact pressure and friction coefficient should be comparable for adult and neonatal RBCs. In the constriction channel, contact area is proportional to RBC volume. Therefore, it is not surprising that transit time as a function of RBC volume can be fitted into a single line for both adult and neonatal, indicating that the transit time difference for adult RBCs and neonatal RBCs were mainly caused by their volume difference.

Conclusion

This paper presented a microfluidic system capable of measuring multiple biophysical parameters on single RBCs. Compared with previously reported microfluidic devices for single RBC biophysical measurement, this system has a higher throughput (100–150 cells s^{-1}), higher signal to noise ratio, and the capability of performing multi-parameter measurements. The microfluidic system may have potential applications in drug efficacy testing and RBC property characterization relevant to clinical conditions. Pattern recognition confirmed that a combination of measurements of transit time, electrical impedance amplitude, and impedance phase resulted in a high success rate in classifying fetal/neonatal and adult RBCs. However, the achieved 89.2% specificity and 80.2% sensitivity for cell classification require further improvement for diagnostics applications such as rare fetal RBC enumeration in adult blood.

Acknowledgements

References

1 R. Skalak and P. I. Branemark, Deformation of Red Blood Cells in Capillaries, *Science*, 1969, **164**, 717.

2 A. W. L. Jay, Viscoelastic Properties of The Human Red Blood Cell Membrane. I. Deformation, Volume Loss, and Rupture of Red Cells in Micropipettes, *Biophys. J.*, 1973, **13**, 1166–1182.

3 P. R. Zarda, *et al.*, Elastic Deformations of Red Blood-Cells, *J. Biomech.*, 1977, **10**, 211–221.

4 A. Iglic, *et al.*, Depletion of Membrane Skeleton in Red-Blood-Cell Vesicles, *Biophys. J.*, 1995, **69**, 274–279.

5 M. Diez-Silva, *et al.*, Shape and Biomechanical Characteristics of Human Red Blood Cells in Health and Disease, *MRS Bull.*, 2010, **35**, 382–388.

6 O. K. Baskurt, *et al.*, Red Blood Cell Deformability in Sepsis, *American Journal of Respiratory and Critical Care Medicine*, 1998, **157**, 421–427.

7 T. C. Hurd, *et al.*, Red Blood-Cell Deformability in Human and Experimental Sepsis, *Arch. Surg.*, 1988, **123**, 217–220.

8 H. Bow, *et al.*, A Microfabricated Deformability-Based Flow Cytometer with Application to Malaria, *Lab Chip*, 2011, **11**, 1065–1073.

9 J. P. Shelby, *et al.*, A Microfluidic Model for Single-Cell Capillary Obstruction by Plasmodium Falciparum Infected Erythrocytes, *Proc. Natl. Acad. Sci. U. S. A.*, 2003, **100**, 14618–14622.

10 G. A. Barabino, *et al.*, Sickle Cell Biomechanics, *Annu. Rev. Biomed. Eng.*, 2010, **12**, 345–367.

11 S. K. Ballas and E. D. Smith, Red-Blood-Cell Changes during the Evolution of the Sickle-Cell Painful Crisis, *Blood*, 1992, **79**, 2154–2163.

12 J. Bhavsar and R. S. Rosenson, Adenosine Transport, Erythrocyte Deformability and Microvascular Dysfunction: An Unrecognized Potential Role for Dipyridamole Therapy, *Clinical Hemorheology and Microcirculation*, 2010, **44**, 193–205.

13 S. A. Desai and R. L. Rosenberg, Pore Size of The Malaria Parasite's Nutrient Channel, *Proc. Natl. Acad. Sci. U. S. A.*, 1997, **94**, 2045–2049.

14 A. B. Vaidya, Malaria Parasites Deck The Holes in Erythrocytes, *Blood*, 2004, **104**, 3844–3844.

15 S. M. Huber, *et al.*, Chloride Conductance and Volume-Regulatory Nonselective Cation Conductance in Human Red Blood Cell Ghosts, *Pfluegers Arch.*, 2001, **441**, 551–558.

16 S. A. Desai, *et al.*, A Voltage-Dependent Channel Involved in Nutrient Uptake by Red Blood Cells Infected with The Malaria Parasite, *Nature*, 2000, **406**, 1001–1005.

17 D. H. Kim, *et al.*, Microengineered Platforms for Cell Mechanobiology, *Annu. Rev. Biomed. Eng.*, 2009, **11**, 203–233.

18 Y. Zheng and Y. Sun, Microfluidic Devices for Mechanical Characterisation of Single Cells in Suspension, *Micro Nano Lett.*, 2011, **6**, 327–331.

19 R. M. Hochmuth, Micropipette Aspiration of Living Cells, *J. Biomech.*, 2000, **33**, 15–22.

20 S. Sen, *et al.*, Indentation and Adhesive Probing of A Cell Membrane with AFM: Theoretical Model and Experiments, *Biophys. J.*, 2005, **89**, 3203–3213.

21 T. G. Kuznetsova, *et al.*, Atomic Force Microscopy Probing of Cell Elasticity, *Micron*, 2007, **38**, 824–833.

22 S. Suresh, *et al.*, Connections between Single-Cell Biomechanics and Human Disease States: Gastrointestinal Cancer and Malaria, *Acta Biomater.*, 2005, **1**, 15–30.

23 R. P. Huruta, *et al.*, Mechanical Properties of Stored Red Blood Cells Using Optical Tweezers, *Blood*, 1998, **92**, 2975–2977.

24 M. Abkarian, *et al.*, High-Speed Microfluidic Differential Manometer for Cellular-Scale Hydrodynamics, *Proc. Natl. Acad. Sci. U. S. A.*, 2006, **103**, 538–542.

25 J. Wan, *et al.*, Dynamics of Shear-Induced ATP Release from Red Blood Cells, *Proc. Natl. Acad. Sci. U. S. A.*, 2008, **105**, 16432–16437.

26 G. Tomaiuolo, *et al.*, Microfluidics Analysis of Red Blood Cell Membrane Viscoelasticity, *Lab Chip*, 2011, **11**, 449–454.

27 N. Bao, *et al.*, Single-Cell Electrical Lysis of Erythrocytes Detects Deficiencies in The Cytoskeletal Protein Network, *Lab Chip*, 2011, **11**, 3053–3056.

28 X. H. Li, *et al.*, Microfluidic System for Planar Patch Clamp Electrode Arrays, *Nano Lett.*, 2006, **6**, 815–819.

29 K. C. Tang, *et al.*, Lateral Patch-Clamping in A Standard 1536-Well Microplate Format, *Lab Chip*, 2010, **10**, 1044–1050.

30 M. Khine, *et al.*, A single cell electroporation chip, *Lab Chip*, 2005, **5**, 38–43.

31 A. Y. Lau, *et al.*, Open-Access Microfluidic Patch-Clamp Array with Raised Lateral Cell Trapping Sites, *Lab Chip*, 2006, **6**, 1510–1515.

32 R. Georgieva, *et al.*, Low Frequency Electrorotation of Fixed Red Blood Cells, *Biophys. J.*, 1998, **74**, 2114–2120.

33 J. Yang, *et al.*, Dielectric Properties of Human Leukocyte Subpopulations Determined by Electrorotation as A Cell Separation Criterion, *Biophys. J.*, 1999, **76**, 3307–3314.

34 D. Holmes, *et al.*, Leukocyte Analysis and Differentiation Using High Speed Microfluidic Single Cell Impedance Cytometry, *Lab Chip*, 2009, **9**, 2881–2889.

35 C. Bernabini, *et al.*, Micro-Impedance Cytometry for Detection and Analysis of Micron-Sized Particles and Bacteria, *Lab Chip*, 2011, **11**, 407–412.

36 A. Valero, *et al.*, A Unified Approach to Dielectric Single Cell Analysis: Impedance and Dielectrophoretic Force Spectroscopy, *Lab Chip*, 2010, **10**, 2216–2225.

37 K. Cheung, *et al.*, Impedance Spectroscopy Flow Cytometry: On-Chip Label-Free Cell Differentiation, *Cytometry, Part A*, 2005, **65A**, 124–132.

38 J. Chen, *et al.*, A Microfluidic Device for Simultaneous Electrical and Mechanical Measurements on Single Cells, *Biomicrofluidics*, 2011, **5**, 014113.

39 T. Sun and H. Morgan, Single-Cell Microfluidic Impedance Cytometry: A Review, *Microfluid. Nanofluid.*, 2010, **8**, 423–443.

40 K. C. Cheung, *et al.*, Microfluidic Impedance-Based Flow Cytometry, *Cytometry, Part A*, 2010, **77A**, 648–666.

41 D. R. Gossett, *et al.*, Deformability Cytometry: High-Throughput, Continuous Measurement of Cell Mechanical Properties in Extesional Flow," presented at the Proc. of the Int. Conf. on Miniaturized Systems for Chemistry and Life Sciences 2010 (MicroTAS 2010), Groningen, The Netherlands, 3–7 October, 2010.

42 J. Chen, *et al.*, Classification of Cell Types Using A Microfluidic Device for Mechanical and Electrical Measurement on Single Cells, *Lab Chip*, 2011, **11**, 3174–3181.

43 F. C. Colin, *et al.*, Impaired Fetal Erythrocytes Filterability - Relationship with Cell-Size, Membrane Fluidity, and Membrane Lipid-Composition, *Blood*, 1992, **79**, 2148–2153.

44 O. Linderkamp, *et al.*, Deformability and Intrinsic Material Properties of Neonatal Red-Blood-Cells, *Blood*, 1986, **67**, 1244–1250.